catalysts

MDPI

Article

Investigation of C_1 + C_1 Coupling Reactions in Cobalt-Catalyzed Fischer-Tropsch Synthesis by a Combined DFT and Kinetic Isotope Study

Yanying Qi, Jia Yang *, Anders Holmen and De Chen *

Department of Chemical Engineering, Norwegian University of Science and Technology, Sem Sælands vei 4, N-7491 Trondheim, Norway; yanying.qi@ntnu.no (Y.Q.); anders.holmen@ntnu.no (A.H.)

* Correspondence: jia.yang@ntnu.no (J.Y.); de.chen@ntnu.no (D.C.)

Received: 2 June 2019; Accepted: 17 June 2019; Published: 19 June 2019

Abstract: Understanding the chain growth mechanism is of vital importance for the development of catalysts with enhanced selectivity towards long-chain products in cobalt-catalyzed Fischer-Tropsch synthesis. Herein, we discriminate various C_1 + C_1 coupling reactions by theoretical calculations and kinetic isotope experiments. $CH_{x(x=0-3)}$, CO, HCO, COH, and HCOH are considered as the chain growth monomer respectively, and 24 possible coupling reactions are first investigated by theoretical calculations. Eight possible C_1 + C_1 coupling reactions are suggested to be energetically favorable because of the relative low reaction barriers. Moreover, five pathways are excluded where the C_1 monomers show low thermodynamic stability. Effective chain propagation rates are calculated by deconvoluting from reaction rates of products, and an inverse kinetic isotope effect of the C_1 + C_1 coupling reaction is observed. The theoretical kinetic isotope effect of CO + CH_2 is inverse, which is consistent with the experimental observation. Thus, the CO + CH_2 pathway, owing to the relatively lower barrier, the high thermodynamic stability, and the inverse kinetic isotope effect, is suggested to be a favorable pathway.

Keywords: Fischer-Tropsch synthesis; chain growth; CO insertion; kinetic isotope effect; DFT

1. Introduction

Fischer-Tropsch synthesis (FTS) is an alternative process to produce clean liquid fuels by converting syngas [1–4]. Cobalt-based catalysts, owing to the low water-gas shift activity and the remarkable stability, are favorable catalysts, for the synthesis of long-chain hydrocarbons from the synthesis gas with an H_2/CO ratio of about 2 [5–7]. Understanding the reaction mechanisms of chain propagation and termination of cobalt-catalyzed FTS is crucial to achieve a high selectivity of long-chain hydrocarbons. Considerable efforts have contributed to the investigation of the reaction mechanisms, and three prevailing mechanisms are proposed [8–15], that is, carbide mechanism, hydroxycarbene mechanism, and CO insertion mechanism. However, there is still no consensus about the chain growth mechanism because of the complexity of FTS reaction system.

The carbide mechanism was originally proposed by Fischer and Tropsch [16], suggesting that CO adsorbs dissociatively on the catalyst surface and the surface carbon is subsequently hydrogenated to form a methylene (CH_2) group, which is considered as a chain propagation monomer. The experimental results from Brady and Pettit [17,18] demonstrated that only the carbide mechanism could produce the product composition, and other mechanisms were thus excluded. However, an assumption was automatically made in their analysis, where the reactions of CH_2 with O and OH were ignored. Hu and coworkers suggested that CH_3 + C and CH_2 + CH_2 are two major chain growth pathways at step sites based on the calculated reaction rates for all C_1 + C_1 coupling pathways in the carbide

mechanism [19]. Furthermore, coupling reactions of RCH_2 + C and RCH + CH_2 are proposed to be two major pathways for all the hydrocarbons with different carbon numbers [15]. However, the CO/HCO insertion mechanism is not considered in their calculations. The carbide mechanism is also demonstrated to be a favorable pathway on the Co(10−10) surface [20] and Co(10−11) [21] based on density functional theory(DFT) calculations. Recently, steady state isotopic transient kinetic analysis(SSITKA) measurements proved that chain growth rate is much higher compared with the rate of monomer formation [22], which means the rate of monomer formation or the site coverage of monomer need to be taken into account in the discrimination of chain growth mechanisms. Notably, the carbide mechanism cannot account for all the products' formation, especially oxygenates.

As an alternative to the carbide mechanism, the CO insertion mechanism is reported to be a preferred mechanism, considering that its reaction barrier is low on Co(0001) and the theoretical turnover frequency(TOF) fits well with the experimental value [12,23]. Meanwhile, transient kinetic studies between the H_2/inert and H_2/CO forward and backward switch provide an indication of CO involved in the C_{2+} formation [24]. The authors also found that the chain growth probability is proportional to the partial pressure of CO rather than the surface C coverage, which further supports their argument that CO is the chain growth monomer. However, further DFT and experimental studies are needed to distinguish the nature of the monomer, such as CO and CH_xO_y, in the chain growth pathway. The CHO insertion pathway is demonstrated to be more energetically favorable on a clean Co(0001) surface [11]. It is reported that the chain growth proceeds via the CO insertion mechanism on Co(0001) and the stepped surfaces, but via the carbide mechanism on a more open Co(10−11) surface at lower CO coverage [25]. It is noted that the chain growth mechanism is sensitive to both the surface structure and the CO coverage. Thus, the different surface models and CO site coverages employed in the various theoretical calculations result in different conclusions. A considerable debate still remains and, therefore, a systematic comparison of all the possible reaction pathways under certain CO coverage is highly desired.

It is difficult to discriminate reaction mechanisms of complex reaction networks such as FTS by solely employing theoretical or experimental methods. In the current study, a combined approach of kinetic isotope experiments and DFT calculations was employed to study the chain growth mechanism in cobalt-catalyzed Fischer-Tropsch synthesis. The combined method has proved very useful in the mechanism investigation of CO activation and methane formation [26,27]. We firstly calculated the reaction barriers of all the possible coupling reactions with CH_x, CO, HCO, COH, and HCOH as the chain growth monomers by DFT calculations. The thermodynamic stability of C_1 monomers was analyzed to further discriminate various reactions. Moreover, we performed kinetic isotope experiments using H_2 and D_2. The reaction rates of the products were deconvolved to get the effective chain propagation rate, and thus the kinetic isotope effect (KIE) of the C_1 + C_1 coupling reaction was obtained. Kinetic isotope effects of the energetically favorable pathways were calculated and compared with the experimental result to further identify the favorable reaction pathway.

2. Results and Discussion

2.1. Adsorption of C_2 Species

The adsorption characteristics of C_2 surface species involved in the reaction were first evaluated. The most stable adsorption configurations are summarized in Figure 1, and the corresponding adsorption energies and structural parameters are reported in Table 1. The favorable adsorption site of CO was the top site, which is consistent with the experimental observation [28,29]. It is noted that one CO spectator is clearly seen in Figure 1, while the other CO spectator is covered by the inserted side view. The detailed positions of the CO spectators are shown in Figure S1, Supplementary Materials. For C-$CH_{x(x=0-3)}$ species, the carbon atom adsorbs on the hcp hollow site and $CH_{x(0-2)}$ bonds to the nearby fcc/top site, while CH_3 points away from the surface. CH adsorbs on the fcc hollow site in CH-$CH_{x(x=1-3)}$ species. The distance between two carbon atoms increases with an increasing x value

in C (CH, CH_2, CO, HCO, COH, or HCOH)-$CH_{x(x=1-3)}$. For most oxygenates, CH_x prefers to adsorb on the hollow site. The C-C distances are similar for the same x value in the different surface species $CH_{x(1-3)}$-CO(HCO, COH, HCOH). The adsorption energies of most surface species are slightly smaller compared with the literature values, which could be the result of different functional and CO site coverage employed. The adsorption energies of CH_2CO and CH_2HCO calculated by employing Perdew-Burke-Ernzerhof functional are −0.85 eV and −2.12 eV, respectively, which are similar to the literature values of −0.98 eV and −2.18 eV, respectively [23].

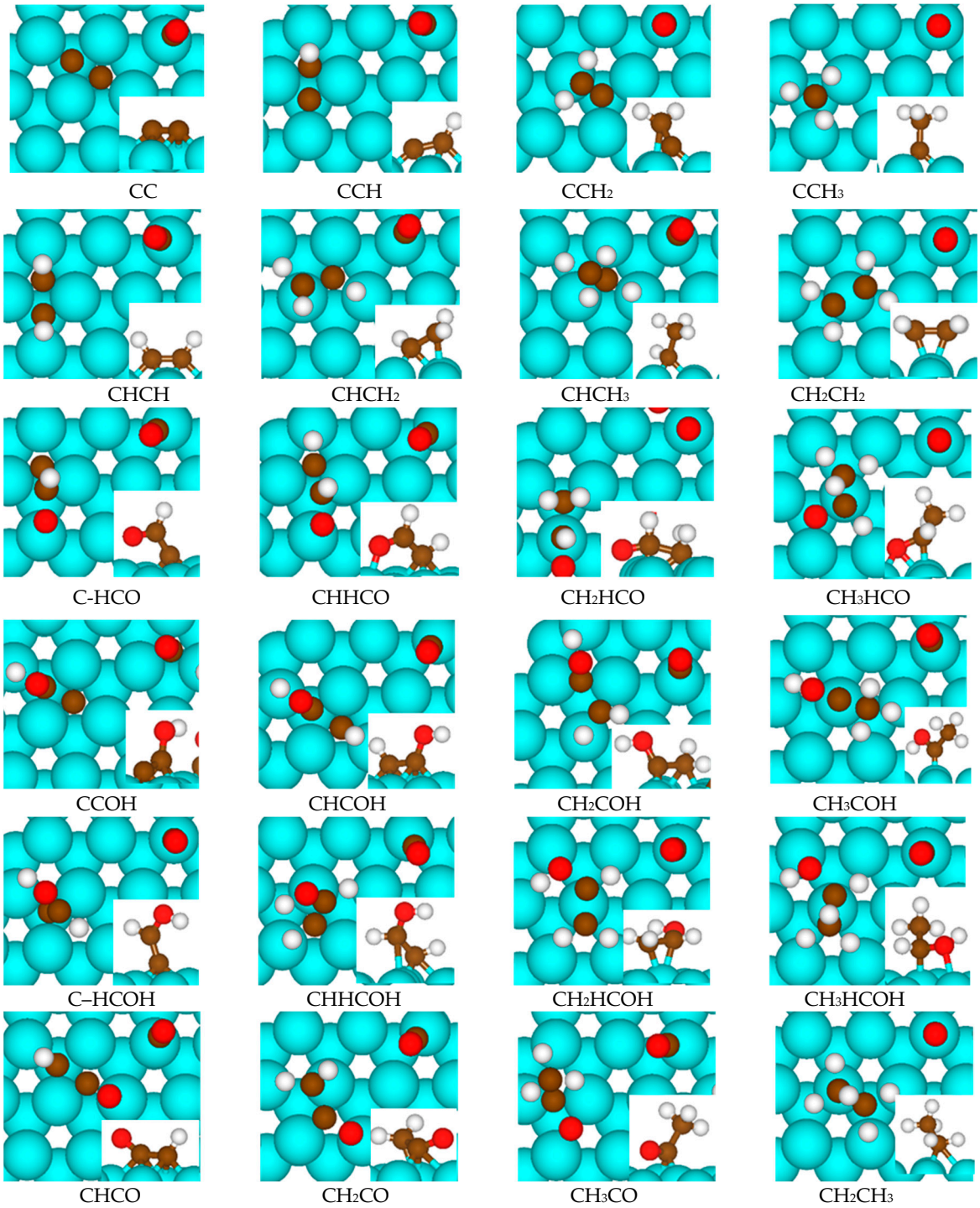

Figure 1. Top views and side views (inserted) of C_2 species adsorbed on the surface.

Table 1. Adsorption energies and structure parameters of C_2 species.

Surface Species	E_{ads} (eV)	d_{C-C} (Å)	d_{C-O} (Å)	d_{C-H} (Å)
CC	−6.49	1.33	–	–
CCH	−4.83	1.35	–	1.09
CCH_2	−3.68	1.38		1.09
CCH_3	−5.13	1.50		1.10
CHCO	−2.82	1.39	1.25	1.09
CH_2CO	−0.77	1.43	1.28	1.09
CH_3CO	−1.86	1.51	1.31	1.10
CHCH	−2.12	1.38		1.09
$CHCH_2$	−2.46	1.41		1.09
$CHCH_3$	−3.35	1.52		1.15, 1.09
CH_2CH_2	−0.77	1.42		1.09
CH_2CH_3	−1.44	1.55		1.10
CH_3CH_3	−0.35	1.53		1.09
C-HCO	−4.67	1.42	1.28	1.10
CHHCO	−3.96	1.41	1.29	1.10
CH_2HCO	−2.01	1.43	1.19	1.04
CH_3HCO	−0.59	1.50	1.35	1.09
C-COH	−4.79	1.39	1.34	–
CHCOH	−2.01	1.41	1.37	1.09
CH_2COH	−2.34	1.45	1.35	1.09
CH_3COH	−2.36	1.50	1.34	1.09
C-HCOH	−4.43	1.38	1.34	1.09
CHHCOH	−2.77	1.39	1.35	1.11
CH_2HCOH	−0.65	1.40	1.38	1.09
CH_3HCOH	−1.43	1.52	1.46	1.10

2.2. DFT Calculations of C_1 + C_1 Coupling Reactions

The most favorable pathway of CO activation is the hydrogenation-assisted CO dissociation on Co(0001), according to the previous results [26,27,30,31]. Herein, the intermediates such as CH_x, CO, HCO, COH, and HCOH were considered as the chain growth monomer, respectively. The transition states were located for the coupling reactions involving CH_x, CO, HCO, COH, and HCOH.

The configurations of the transition states are plotted in Figure 2 and the reaction barriers are summarized in Table 2, where the vertical row is arranged by the sequence of the intermediates in the reaction from syngas towards methane and the horizontal row is the possible intermediates involved in the reactions. For the transition states of coupling reactions between C and $CH_{x(0-3)}$, the C atom always bonds to the hcp hollow site and the $CH_{x(0-3)}$ bonds to the nearby bridge or top site, which is consistent with the results reported by Cheng et al. [19]. With respect to the coupling reactions CH + CH, CH + CH_2, CH + CH_3, CH_2 + CH_2, and CH_2 + CH_3, CH and CH_2 adsorb on the hollow sites. For CO, HCO, COH, and HCOH insertion reactions, C, CH, and CH_2 adsorb on the hollow sites, while CH_3 bonds to the off-top site. The barrier of the C + C coupling reaction (i.e., 0.97 eV) is the highest and that of C + CH_2 is the lowest among all the coupling reactions between C and $CH_{x(0-3)}$. The barriers of C + CH, C + CH_3, CH + CH_3, and CH_2 + CH_3 are around 0.70 eV. It is noted that the barrier of CH_2 + CH_2 (i.e., 0.12 eV) is the lowest, while that of CH_3 + CH_3 (i.e., 1.84 eV) is the highest among all the $CH_{x(0-3)}$ + $CH_{x(0-3)}$ coupling reactions. For the CO insertion reactions, the barrier of the CH_3 + CO coupling reaction (i.e., 1.19 eV) is higher than the others, which is attributed to the strong and directional CH_3 surface bonds, as reported previously [12]. The CH_2 + CO coupling shows the lowest barrier (i.e., 0.56) among all the CO insertion pathways. With regards to HCO insertion into CH_x, the barriers are lower than the corresponding CO insertion reactions, and thus the HCO insertion is more favourable over the CO insertion by solely comparing the reaction barriers. The smaller gap between the highest occupied molecular orbital and the lowest unoccupied molecular orbital of HCO compared with that of CO greatly facilitates the charge transfer and hybridization between HCO and

catalysts, as reported by Li and co-workers [11], which results in the higher activity of HCO insertion. The relative barriers of HCO insertion reactions follow a similar pattern to the CO insertion pathways, and the barrier of CH_3 + HCO is the largest. CH_2 + HCO owns a significantly lower barrier, which is 0.05 eV. For COH insertion into CH_x, the barriers are higher than that for HCO insertion because of the relatively strong adsorption of COH. The pathways of HCOH insertion into CH_x also exhibit low barriers, especially for HCOH + CH_2.

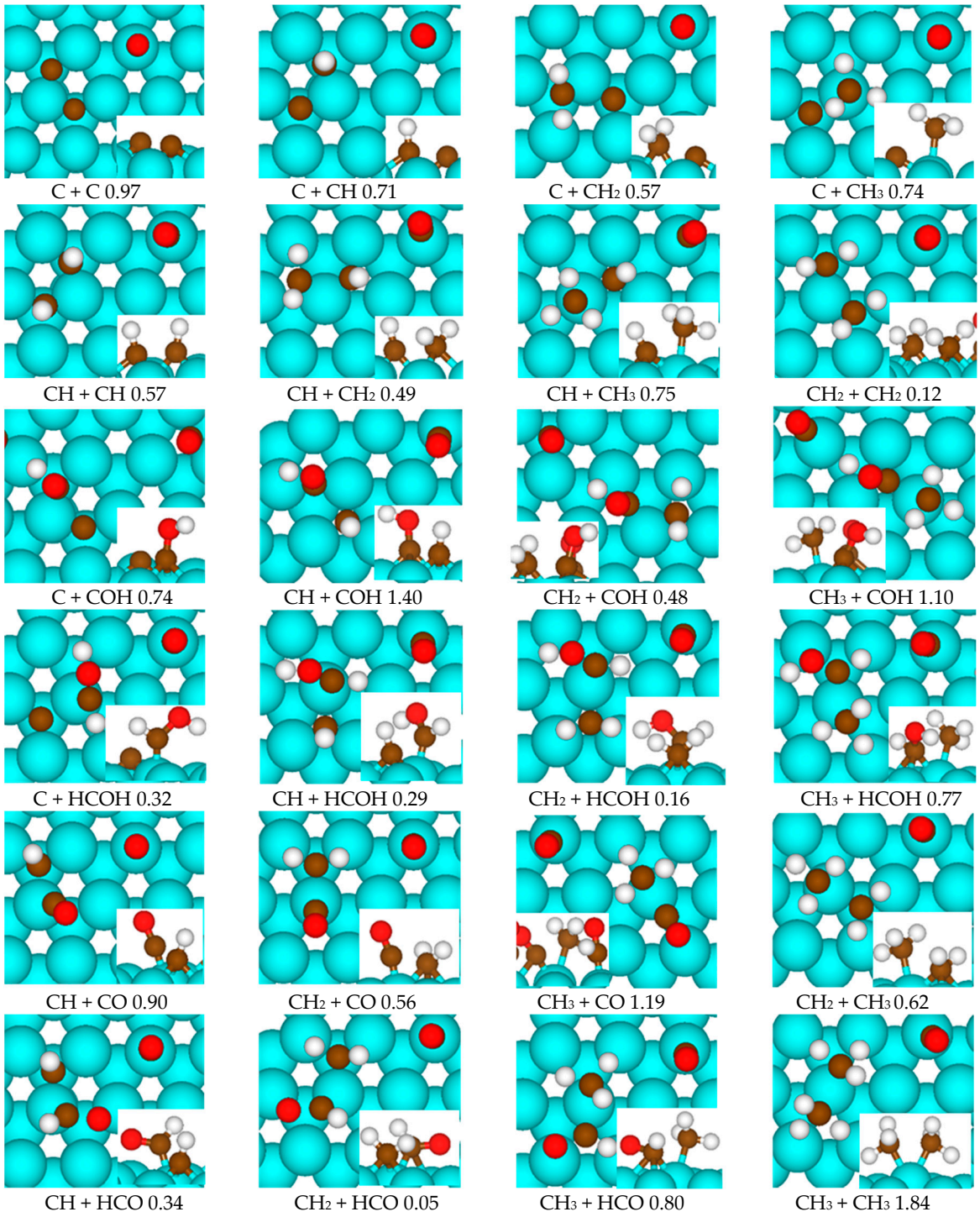

Figure 2. Top views and side views (inserted) of transition states for the C_1 + C_1 coupling reactions. The number represents the activation energy in eV.

Table 2. Activation energies of the coupling reactions.

	+CO	**+HCO**	**+HCOH**	**+CH**	**+CH_2**	**+CH_3**	**+C**	**+COH**
HCO	–	–	–	0.34	0.05	0.80	–	–
HCOH	–	–	–	0.29	0.16	0.77	0.32	–
CH	0.90	0.34	0.29	0.57	0.49	0.75	0.71	1.40
CH_2	0.56	0.05	0.16	0.49	0.12	0.62	0.57	0.48
CH_3	1.19	0.80	0.77	0.75	0.62	1.84	0.74	1.10

The barriers of coupling reactions are summarized in a special style in Table 3, where both vertical and horizontal rows are in an order of low to high adsorption heat of the intermediates. It clearly shows that the central area of the table gives the lower activation energies, which possibly suggests that there is a volcano curve between the activation barriers and the adsorption energies. For the steps between HCO and HCOH, the transition states are difficult to locate. Besides, the site coverage of HCOH is low because the hydrogenation of HCO is rate determining [26,27]. Considering the low site coverage of HCOH, the activity of the steps involving HCOH will be low, and thus these steps are not favorable.

Table 3. Comparison of the activation energies of main coupling reactions.

	CH_3	**HCO**	**HCOH**	**CH_2**	**CH**
CH_3	1.84	0.80	0.77	0.62	0.75
HCO	0.80	–	–	0.05	0.34
HCOH	0.77	–	–	0.16	0.29
CH_2	0.62	0.05	0.16	0.12	0.49
CH	0.75	0.34	0.29	0.49	0.57

By analyzing the activation barriers, the reactions with CH_3 display relative high barriers compared with other CH_x species, and thus we exclude the possibility with CH_3 participating in the chain growth mechanism. We estimate that an increase of the barrier by 0.1 eV could roughly result in a decrease of reaction rate by an order of magnitude at 500 K, when keeping the site coverages of surface species constant. Thus, we could also exclude the reactions with barriers larger than 0.6 eV. As we know, the reaction rate of a surface reaction is a combined result from the reaction barrier and the site coverage of reactants. We exclude the possibility of HCOH as a chain initiator or monomer considering the low site coverage of HCOH. Therefore, the remaining possibilities are as follows: CO + CH_2, HCO + CH, HCO + CH_2, CH + CH, CH + CH_2, CH_2 + CH_2, C + CH_2, and CH_2 + COH.

2.3. Thermodynamic Analysis

The thermodynamic stability of the possible chain growth monomers is another important factor to identify the favourable reaction mechanism. Figure 3 illustrates the relative free energy of each C_1 monomer at 483 K with the pressure at 1.85 bar and 20 bar, respectively. The calculation details are summarized in S1, Supplementary Materials. We can get a clear understanding of which species are likely to be present on the cobalt surface by analysing the relative free energies. HCOH is the most unstable one, which is expected. CO is the most stable one, which is consistent with the SSITKA result, observing the CO coverage of 0.5 [26]. The relative free energy decreases with the increase of the pressure, which means the adsorption of CO is stronger and the site coverage of CO is larger at a higher pressure. The combined relative free energy of two reactants for the eight energetic favourable C_1 + C_1 reactions are summarized in Table 4. The CO + CH_2 coupling reaction shows extremely high thermodynamics stability, owing to the low free energy of CO. The relative free energy reflects the thermodynamic stability of the reactants and the high value indicates thermodynamic instability, and thus will be unlikely present under the reaction condition. Thus, we exclude the coupling reactions involving C_1 species with relatively low thermodynamic stability and select three

C–C coupling reactions with low relative free energy (i.e., CO + CH_2, HCO + CH, CH + CH) to be further discriminated by the analysis of kinetic isotope effect.

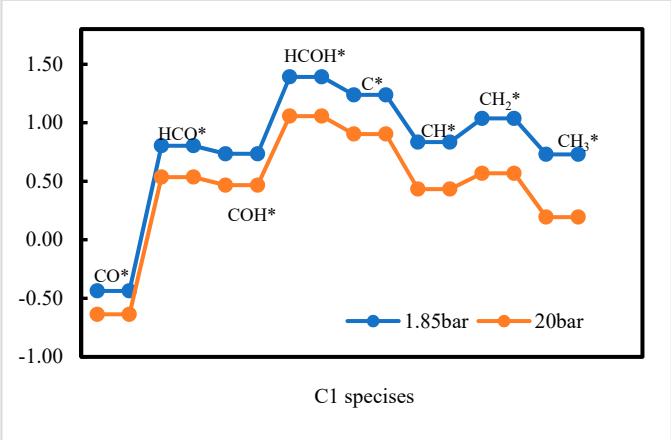

Figure 3. Free energies of each C_1 monomer, referenced to CO(g), H_2O(g), and H_2(g) for Fischer-Tropsch synthesis at the pressure of 1.85 bar and 20 bar with H_2/CO = 2 and 483 K.

Table 4. The combined relative free energies of two reactants.

Reactants	CO + CH_2	HCO + CH	HCO + CH_2	CH + CH	CH + CH_2	CH_2 + CH_2	C + CH_2	CH_2 + COH
G(eV)	0.60	1.64	1.84	1.67	1.87	2.07	2.28	1.77

2.4. *Analysis of Kinetic Isotope Effect*

The kinetic isotope effect (KIE) is defined as the ratio of the rates with CO/H_2 and CO/D_2 as reactants (r_H/r_D), which could provide important kinetic information, assisting in the discrimination of reaction mechanisms. The KIE was measured for the product formation on a 20% Co/CNT catalyst, as shown in Table 5. The product with a certain carbon number (C_n) includes both olefin and paraffin products.

Table 5. Kinetic isotope effects (KIE) for the product formation (483 K, 1.85 bar, H_2/CO = D_2/CO = 10).

Reaction Rate [μmol/(g_{cat}s)]	$r_{t,H}$	$r_{t,D}$	KIE = $r_{t,H}/r_{t,D}$
r_{CH4}	2.349	2.383	0.99
r_{C2}	0.158	0.180	0.88
r_{C3}	0.128	0.192	0.66
r_{C4}	0.076	0.152	0.50
r_{C5+}	0.046	0.121	0.38

The magnitude of inverse KIE increases with an increasing carbon number, as shown in Table 5. To study the chain growth step by monomer addition, an effective chain propagation rate is introduced and its KIE is investigated. Scheme 1 describes a simplified reaction network in this study.

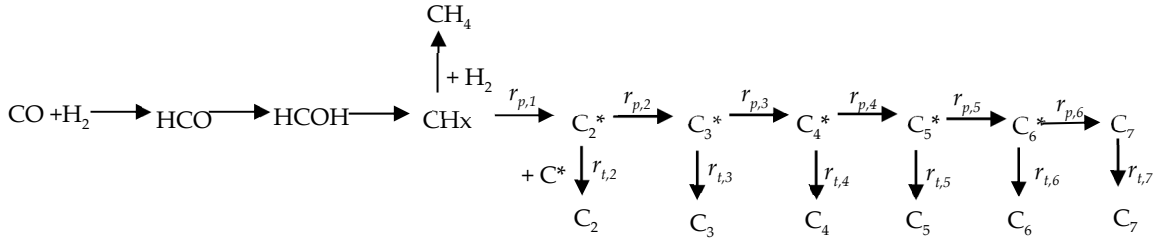

Scheme 1. Reaction network of cobalt-catalyzed Fischer-Tropsch synthesis.

The effective chain propagation rate ($r_{p,n}$) is calculated in such a way that the effect of the chain propagation reaction after particular carbon number (C_7) is excluded owing to methanation conditions, as shown in Equations (1) and (2).

$$r_{p,6} = r_{t,7} \tag{1}$$

$$r_{p,n} = r_{t,n+1} + \frac{n+1}{n+2} r_{p,n+1}, n = 1\text{–}5, \tag{2}$$

where $r_{t,n}$ and $r_{p,n}$ are the carbon based termination and propagation rate, respectively, of the hydrocarbon with carbon number n. According to the equations, we can get the $r_{p,n}$ with CO/H_2 and CO/D_2 as reactants, and the results are summarized in Table 6. The KIE values for the propagation reactions decrease with the increasing carbon number. A similar phenomenon was observed for CO_2 hydrogenation on both Co and Fe catalysts [32].

Table 6. Kinetic isotope effects for the propagation rate with different carbon numbers (483 K, 1.85 bar, $H_2/CO = D_2/CO = 10$).

Reaction Rate [mol/(g_{cat}s)]	r_H	r_D	KIE
$r_{p,4}$	0.05	0.12	0.38
$r_{p,3}$	0.11	0.25	0.45
$r_{p,2}$	0.21	0.38	0.56
$r_{p,1}$	0.30	0.43	0.69

An inverse KIE (i.e., 0.69) of the $C_1 + C_1$ coupling reaction is observed experimentally. It is generally assumed that the KIE is expressed as the difference in rate constants in the calculations, which involves the contribution from the zero-point energy (ZPE) differences and the entropy differences (ΔS) between H and D isotopic isomers. The details of KIE calculation are reported in S2, Supplementary Materials [27,31]. The results of different coupling reactions are summarized in Table 7. The KIEs of three possible coupling reactions are 0.84, 0.98, and 0.95 for $CH_2 + CO$, $CH + HCO$, and $CH + CH$ at 500 K, respectively. $CO + CH_2$ shows inverse KIE, which is mainly attributed to the contribution of zero-point energy. The differences of KIE between the theoretical calculation and the experimental observation could be attributed to the accuracy of second-derivation methods to estimate the vibrational frequency [31]. Small inaccuracy in theoretical calculations may result in deviation of the kinetic isotope effect, as KIE is highly sensitive to vibrational frequencies. Besides, the catalyst surface is more complicated than the model employed. The KIEs of $CH + HCO$ and $CH + CH$ are around 1, which do not show inverse isotope effects and could be excluded. Therefore, $CO + CH_2$ could be the possible reaction pathway owing to its reverse kinetic isotope effect.

Table 7. The kinetic isotope effect at 500 K for three possible coupling routes.

Elementary Step	ZPE Contribution	Entropic Contribution	KIE
$CO + CH_2 \rightarrow CH_2CO$	0.78	1.08	0.84
$HCO + CH \rightarrow CHHCO$	0.96	1.02	0.98
$CH + CH \rightarrow CHCH$	0.91	1.04	0.95

3. Method

3.1. Theoretical Method and Model

All DFT calculations were implemented with the Vienna Ab initio Simulation Package (VASP) [33] using Bayesian error estimation functional with van der Waals correlation (BEEF-vdW) [34] and projector augmented wave (PAW) pseudopotentials [35]. Spin polarization was involved in all calculations. Large-sized Co nanoparticles were used in our experiments. On the basis of a geometrical, cuboctahedral model from Van Hardeveld and Hartog, terrace surfaces are dominant for large particles [36]. Besides,

the (111) face-centered-cubic (fcc)-cobalt is detected in the X-ray powder diffraction pattern and the high-resolution transmission electron microscopy image of reduced cobalt-based catalysts [37]. The Co(0001) surface of hexagonal close-packed (hcp) is close to the (111) surface of fcc metals. Therefore, Co(0001) was selected as the model. A 3×3 supercell of five layers and 12 Å of vacuum spacing between the successive metal slabs was used. Two CO molecules were pre-adsorbed on the surface as spectators in this work. An electronic plane wave cut-off of 500 eV was used, with the Brillouin zone being sampled by a mesh of $5 \times 5 \times 1$. For the Fermi-surface smearing, the first-order Methfessel–Paxton scheme was applied with a smearing width of 0.2 eV. The nudged elastic band (NEB) method [38] was employed to locate the initial transition states, which were subsequently optimized by the dimer method [39]. Vibrational frequencies were calculated to verify the transition states, with one negative mode corresponding to the desired reaction coordinate. The optimizations were converged until all forces on the atoms were lower than 0.01 eV/Å.

$$E_{ads} = E_{A+slab} - E_A - E_{ads}$$

$$E_a = E_{TS} - E_{IS}$$

Adsorption energies of surface species were defined as the difference between the minimum total energy of the surface species on the slab and total energy of surface plus gas phase species. Activation energies of elementary steps were calculated as the energy difference between the transition states and the separately adsorbed reactants.

Kinetic isotope effects have contributions from zero-point energy (*ZPE*) corrections and entropies (*S*) (see details in S2, Supplementary Materials). For adsorbed species, the frustrated translational and rotational modes are treated as special cases of vibrational modes. Accordingly, the entropy is evaluated by the following:

$$S = S_{vib} = R \sum_{i}^{3N} \left(\frac{x_i}{e^{x_i} - 1} - ln(1 - e^{-x_i}) \right),$$

where $x_i = \frac{hc}{k_B T} \frac{1}{\lambda_i}$, c is speed of light, k_B is Boltzmann constant, and $1/\lambda_i$ is the wavenumber corresponding to each vibrational frequency. Zero-point energies were calculated according to the following equation:

$$E_{ZPE} = \sum_{i=1}^{3N-6(5)} \frac{N_A h v_i}{2},$$

where N_A is Avogadro's number, h is Plank's constant, v_i is the frequency of the normal mode, and N is the number of atoms. All of the frequencies, except those for two CO* spectators and the imaginary one for the transition state, were accounted for by the ZPE and entropy calculations. Vibrational frequencies were calculated by numerical differentiation of the forces using a second-order finite difference approach with a step size of 0.015 Å. The frequencies were converged with respect to the step size. The frequencies are summarized in Table S1, Supplementary Materials. It is reported that the frustrated rotation and translation are with low frequency modes, and those modes contribute largely to the entropy; thus, they need to be computed accurately [40]. Besides, small vibrational frequencies combined with high temperatures could result in larger errors from the harmonic oscillator approximation, as reported by Bai et.al [41]. Most of the frequencies calculated here are larger than 200 cm^{-1} and for these cases, the harmonic oscillator approximation is reasonably accurate.

3.2. Kinetic Isotope Experiment

A 20% Co/CNT (carbon nanotube) catalyst was tested at methanation conditions (483 K, 1.85 bar, H_2/CO = 10). The details of catalyst preparation and characterization have been published in a previous paper [26]. The experiment was performed using a fixed-bed quartz reactor (4 mm i.d.).

The catalyst (25 mg; 53–90 μm) was diluted with 50 mg of inert silicon carbide (75–150 μm) to improve the isothermal conditions along the catalyst bed. The catalyst was reduced in situ in 10 NmL/min H_2 with a ramping rate of 1 K/min to 623 K. After 16 h reduction, the catalyst was cooled down to 443 K. The temperature was then increased at a ramping rate of 1 K/min to 463 K. At 463 K, syngas H_2/CO/Ar (15/1.5/33.5 NmL/min) was introduced and the pressure was adjusted to 1.85 bar. The system was further heated to 483 K at a rate of 1 K/min. The concentrations of H_2, CO, Ar, and C_1–C_7 hydrocarbons were analyzed with an online gas chromatograph (HP5890) equipped with a thermal conductivity detector and a flame ionization detector.

The kinetic isotope effect was determined by switching the feed from H_2/CO to D_2/CO at 483 K, 1.85 bar, and H_2/CO = 10. The kinetic isotope effect measurement was performed after pseudo steady state was reached, about 5 h time on stream.

4. Conclusions

The possible reaction pathways of C_1 + C_1 coupling were firstly explored by calculating the adsorption energies and the activation barriers on the Co(0001) surface with two CO as spectators. The activation energies of the coupling reactions varied from 0.05 eV to 1.84 eV. An increase of the barrier by 0.1 eV could lead to a decrease of reaction rate by an order of magnitude at 500 K, when keeping the site coverages of surface species constant. Thus, we excluded the reactions with barriers larger than 0.6 eV and the remaining possibilities were as follows: CO + CH_2, HCO + CH, HCO + CH_2, CH + CH, CH + CH_2, CH_2 + CH_2, C + CH_2, and CH_2 + COH. It is noted the reaction rate results from both the activation barrier and the site converge of the reactants. The thermodynamic stability of the reactants was analyzed at two different reaction pressures. CO is the most stable specie at both pressures. The chain growth monomers are more stable at a high pressure. Three reaction pathways (i.e., CH_2 + CO, HCO + CH, and CH + CH), with their relatively low barriers and high thermodynamic stability, were further discriminated by analyzing the kinetic isotope effect. Kinetic isotope experiments demonstrated that the magnitude of inverse KIE for the products increases with increasing carbon number. The inverse kinetic isotope effect was observed for the C_1 + C_1 coupling reaction. The theoretical KIE of CH_2 + CO is inverse, which agrees with the experimental result. Therefore, the CH_2 + CO coupling reaction is suggested to be a favorable chain propagation pathway by a combined theoretical calculation and kinetic experiment approach.

Supplementary Materials: The following are available online at http://www.mdpi.com/2073-4344/9/6/551/s1, S1: The calculation method of free energy, Figure S1: The stable configurations of two spectators on the surface, Table S1: Frequencies for the calculation of kinetic isotope effects, S2: The formulas for KIE calculation.

Author Contributions: Conceptualization, Y.Q., J.Y., A.H., and D.C.; methodology, Y.Q., J.Y., A.H., and D.C.; validation, Y.Q. and J.Y.; formal analysis, Y.Q. and J.Y.; investigation, Y.Q. and J.Y.; writing—original draft preparation, Y.Q.; writing—review and editing, Y.Q., J.Y., A.H., and D.C.; supervision, J.Y. and D.C.; funding acquisition, D.C.

Funding: The financial support from Norwegian Research Council through ISP program 209337 and the industrial Catalysis Science and Innovation (iCSI) center is gratefully acknowledged.

Acknowledgments: The computational time provided by the Notur project NN4685K is highly acknowledged.

Conflicts of Interest: The authors declare no conflict of interest.

References

1. Ledesma, C.; Yang, J.; Chen, D.; Holmen, A. Recent Approaches in Mechanistic and Kinetic Studies of Catalytic Reactions Using SSITKA Technique. *ACS Catal.* **2014**, *4*, 4527–4547. [CrossRef]
2. Van Santen, R.A.; Markvoort, A.J.; Filot, I.A.W.; Ghouri, M.M.; Hensen, E.J.M. Mechanism and microkinetics of the Fischer-Tropsch reaction. *Phys. Chem. Chem. Phys.* **2013**, *15*, 17038–17063. [CrossRef] [PubMed]
3. Markvoort, A.J.; van Santen, R.A.; Hilbers, P.A.J.; Hensen, E.J.M. Kinetics of the Fischer-Tropsch Reaction. *Angew. Chem. Int. Ed.* **2012**, *51*, 9015–9019. [CrossRef] [PubMed]
4. Dry, M.E. The Fischer-Tropsch process: 1950–2000. *Catal. Today* **2002**, *71*, 227–241. [CrossRef]

5. Yang, J.; Tveten, E.Z.; Chen, D.; Holmen, A. Understanding the Effect of Cobalt Particle Size on Fischer-Tropsch Synthesis: Surface Species and Mechanistic Studies by SSITKA and Kinetic Isotope Effect. *Langmuir* **2010**, *26*, 16558–16567. [CrossRef]
6. Den Breejen, J.P.; Radstake, P.B.; Bezemer, G.L.; Bitter, J.H.; Froseth, V.; Holmen, A.; de Jong, K.P. On the Origin of the Cobalt Particle Size Effects in Fischer-Tropsch Catalysis. *J. Am. Chem. Soc.* **2009**, *131*, 7197–7203. [CrossRef] [PubMed]
7. Bezemer, G.L.; Bitter, J.H.; Kuipers, H.; Oosterbeek, H.; Holewijn, J.E.; Xu, X.D.; Kapteijn, F.; van Dillen, A.J.; de Jong, K.P. Cobalt particle size effects in the Fischer-Tropsch reaction studied with carbon nanofiber supported catalysts. *J. Am. Chem. Soc.* **2006**, *128*, 3956–3964. [CrossRef] [PubMed]
8. Dry, M.E. Practical and theoretical aspects of the catalytic Fischer-Tropsch process. *Appl. Catal. A Gen.* **1996**, *138*, 319–344. [CrossRef]
9. Roferdepoorter, C.K. A comprehensive mechanism for the Fischer-Tropsch synthesis. *Chem. Rev.* **1981**, *81*, 447–474. [CrossRef]
10. Ledesma, C.; Yang, J.; Blekkan, E.A.; Holmen, A.; Chen, D. Carbon Number Dependence of Reaction Mechanism and Kinetics in CO Hydrogenation on a Co-Based Catalyst. *ACS Catal.* **2016**, *10*, 6674–6686. [CrossRef]
11. Zhao, Y.-H.; Sun, K.; Ma, X.; Liu, J.; Sun, D.; Su, H.-Y.; Li, W.-X. Carbon Chain Growth by Formyl Insertion on Rhodium and Cobalt Catalysts in Syngas Conversion. *Angew. Chem. Int. Ed.* **2011**, *50*, 5335–5338. [CrossRef] [PubMed]
12. Zhuo, M.K.; Tan, K.F.; Borgna, A.; Saeys, M. Density Functional Theory Study of the CO Insertion Mechanism for Fischer-Tropsch Synthesis over Co Catalysts. *J. Phys. Chem. C* **2009**, *113*, 8357–8365. [CrossRef]
13. Inderwildi, O.R.; Jenkins, S.J.; King, D.A. Fischer-tropsch mechanism revisited: Alternative pathways for the production of higher hydrocarbons from synthesis gas. *J. Phys. Chem. C* **2008**, *112*, 1305–1307. [CrossRef]
14. Cheng, J.; Hu, P.; Ellis, P.; French, S.; Kelly, G.; Lok, C.M. Chain growth mechanism in Fischer-Tropsch synthesis: A DFT study of C-C coupling over Ru, Fe, Rh, and Re surfaces. *J. Phys. Chem. C* **2008**, *112*, 6082–6086. [CrossRef]
15. Cheng, J.; Hu, P.; Ellis, P.; French, S.; Kelly, G.; Lok, C.M. A DFT study of the chain growth probability in Fischer-Tropsch synthesis. *J. Catal.* **2008**, *257*, 221–228. [CrossRef]
16. Fischer, F.; Tropsch, H. The Synthesis of Petroleum at Atmospheric Pressures from Gasification Products of Coal. *Brennstoff Chem.* **1926**, *7*, 97–116.
17. Brady, R.C.; Pettit, R. On the mechanism of the Fischer-Tropsch reaction-the chain propagation step. *J. Am. Chem. Soc.* **1981**, *103*, 1287–1289. [CrossRef]
18. Brady, R.C.; Pettit, R. Reactions of diazomethane on transition metal surfaces and their relationship to the mechanism of the Fischer-Tropsch reaction. *J. Am. Chem. Soc.* **1980**, *102*, 6181–6182. [CrossRef]
19. Cheng, J.; Gong, X.Q.; Hu, P.; Lok, C.M.; Ellis, P.; French, S. A quantitative determination of reaction mechanisms from density functional theory calculations: Fischer-Tropsch synthesis on flat and stepped cobalt surfaces. *J. Catal.* **2008**, *254*, 285–295. [CrossRef]
20. Zhang, R.; Kang, L.; Liu, H.; He, L.; Wang, B. Insight into the CC chain growth in Fischer-Tropsch synthesis on HCP Co(10-10) surface: The effect of crystal facets on the preferred mechanism. *Comput. Mater. Sci.* **2018**, *145*, 263–279. [CrossRef]
21. Liu, H.; Zhang, R.; Ling, L.; Wang, Q.; Wang, B.; Li, D. Insight into the preferred formation mechanism of long-chain hydrocarbons in Fischer-Tropsch synthesis on Hcp Co(10-11) surfaces from DFT and microkinetic modeling. *Catal. Sci. Technol.* **2017**, *7*, 3758–3776. [CrossRef]
22. Chen, W.; Filot, I.A.W.; Pestman, R.; Hensen, E.J.M. Mechanism of Cobalt-Catalyzed CO Hydrogenation: 2. Fischer-Tropsch Synthesis. *ACS Catal.* **2017**, *7*, 8061–8071. [CrossRef] [PubMed]
23. Zhuo, M.K.; Borgna, A.; Saeys, M. Effect of the CO coverage on the Fischer-Tropsch synthesis mechanism on cobalt catalysts. *J. Catal.* **2013**, *297*, 217–226. [CrossRef]
24. Schweicher, J.; Bundhoo, A.; Kruse, N. Hydrocarbon Chain Lengthening in Catalytic CO Hydrogenation: Evidence for a CO-Insertion Mechanism. *J. Am. Chem. Soc.* **2012**, *134*, 16135–16138. [CrossRef] [PubMed]
25. Su, H.-Y.; Zhao, Y.; Liu, J.-X.; Sun, K.; Li, W.-X. First-principles study of structure sensitivity of chain growth and selectivity in Fischer-Tropsch synthesis using HCP cobalt catalysts. *Catal. Sci. Technol.* **2017**, *7*, 2967–2977. [CrossRef]

26. Yang, J.; Qi, Y.; Zhu, J.; Zhu, Y.-A.; Chen, D.; Holmen, A. Reaction mechanism of CO activation and methane formation on Co Fischer–Tropsch catalyst: A combined DFT, transient, and steady-state kinetic modeling. *J. Catal.* **2013**, *308*, 37–49. [CrossRef]
27. Qi, Y.; Yang, J.; Duan, X.; Zhu, Y.-A.; Chen, D.; Holmen, A. Discrimination of the mechanism of CH_4 formation in Fischer-Tropsch synthesis on Co catalysts: A combined approach of DFT, kinetic isotope effects and kinetic analysis. *Catal. Sci. Technol.* **2014**, *4*, 3534–3543. [CrossRef]
28. Lahtinen, J.; Vaari, J.; Kauraala, K.; Soares, E.A.; Van Hove, M.A. LEED investigations on Co(0001): The (3 × 3)R30°-CO overlayer. *Surf. Sci.* **2000**, *448*, 269–278. [CrossRef]
29. Lahtinen, J.; Vaari, J.; Kauraala, K. Adsorption and structure dependent desorption of CO on Co(0001). *Surf. Sci.* **1998**, *418*, 502–510. [CrossRef]
30. Ojeda, M.; Nabar, R.; Nilekar, A.U.; Ishikawa, A.; Mavrikakis, M.; Iglesia, E. CO activation pathways and the mechanism of Fischer-Tropsch synthesis. *J. Catal.* **2010**, *272*, 287–297. [CrossRef]
31. Ojeda, M.; Li, A.W.; Nabar, R.; Nilekar, A.U.; Mavrikakis, M.; Iglesia, E. Kinetically Relevant Steps and H-2/D-2 Isotope Effects in Fischer-Tropsch Synthesis on Fe and Co Catalysts. *J. Phys. Chem. C* **2010**, *114*, 19761–19770. [CrossRef]
32. Gnanamani, M.K.; Jacobs, G.; Shafer, W.D.; Sparks, D.; Davis, B.H. Fischer–Tropsch Synthesis: Deuterium Kinetic Isotope Study for Hydrogenation of Carbon Oxides Over Cobalt and Iron Catalysts. *Catal. Lett.* **2011**, *141*, 1420. [CrossRef]
33. Kresse, G.; Furthmuller, J. Efficiency of ab-initio total energy calculations for metals and semiconductors using a plane-wave basis set. *Comput. Mater. Sci.* **1996**, *6*, 15–50. [CrossRef]
34. Wellendorff, J.; Lundgaard, K.T.; Mogelhoj, A.; Petzold, V.; Landis, D.D.; Norskov, J.K.; Bligaard, T.; Jacobsen, K.W. Density functionals for surface science: Exchange-correlation model development with Bayesian error estimation. *Phys. Rev. B* **2012**, *85*, 235149. [CrossRef]
35. Kresse, G.; Joubert, D. From ultrasoft pseudopotentials to the projector augmented-wave method. *Phys. Rev. B* **1999**, *59*, 1758–1775. [CrossRef]
36. Van Hardeveld, R.; Hartog, F. The statistics of surface atoms and surface sites on metal crystals. *Surf. Sci.* **1969**, *15*, 189–230. [CrossRef]
37. Tsakoumis, N.; Dehghan-Niri, R.; Rønning, M.; Walmsley, J.; Borg, Ø.; Rytter, E.; Holmen, A. X-ray absorption, X-ray diffraction and electron microscopy study of spent cobalt based catalyst in semi-commercial scale Fischer-Tropsch synthesis. *Appl. Catal. A Gen.* **2014**, *479*, 59–69. [CrossRef]
38. Jonsson, H.; Mills, G.; Jacobsen, K.W. Nudged elastic band method for finding minimum energy paths of transitions. In *Classical and Quantum Dynamics in Condensed Phase Simulations*; World Scientific: Singapore, 2011; pp. 385–404.
39. Henkelman, G.; Jonsson, H. A dimer method for finding saddle points on high dimensional potential surfaces using only first derivatives. *J. Chem. Phys.* **1999**, *111*, 7010–7022. [CrossRef]
40. Gunasooriya, G.T.K.K.; van Bavel, A.P.; Kuipers, H.P.C.E.; Saeys, M. CO adsorption on cobalt: Prediction of stable surface phases. *Surf. Sci.* **2015**, *642*, 6–10. [CrossRef]
41. Bai, Y.; Chen, B.W.J.; Peng, G.; Mavrikakis, M. Density functional theory study of thermodynamic and kinetic isotope effects of H_2/D_2 dissociative adsorption on transition metals. *Catal. Sci. Technol.* **2018**, *8*, 3321–3335. [CrossRef]